Satélite de Calibración para Experimentos Ultrasensibles de la Polarización del Fondo Cósmico de Microondas desde Tierra

Calibration Satellite for Ultra-sensitive Cosmic Microwave Background Polarization Ground-based Experiments

Trabajo de Fin de Master para acceder al

Master en Física de Partículas y del Cosmos

Autor: Luis Fernando Mejía Jirón
Director: Francisco Javier Casas Reinares

September 18, 2022

Contents

Abstract

In this work, the implementation of a calibration satellite called CalSat is proposed . This mission will be flying in a low earth orbit (LEO) in a sun-synchronous orbit (SSO), and is designed to support ground-based experiments looking for B-modes polarization signals in the cosmic microwave background (CMB). CalSat will emit a series of known polarized signals in order to calibrate experiments looking for the CMB polarization B-modes. Given their weakness, these experiments need a robust calibration processes in order to detect them. The celestial sources utilized nowadays to these calibrations, are not well characterized, which has direct impact on measurement uncertainties. The proposed calibration source on CalSat will be composed of three center frequencies, at 40, 90 and 150 GHz, which are frequencies of interest in the search of the expected B-modes. CalSat will improve the instrumental accuracy, which will facilitate the detection of the expected B-mode polarized signals, for instance reducing the polar angle error to the level of 1 arc-minute. In addition, given the proposed calibration strategy, CalSat will count with optimal visibility for ground-based experiments located in Atacama and Tenerife. Finally, our results about the thermal control, determine that CalSat will not saturate any studied experiment due to the thermal emission.

Resumen

En este trabajo se propone la implementación de un satélite de calibración llamado CalSat. Esta misión volará en una órbita terrestre baja (LEO) en una órbita heliosincrónica (SSO), y está diseñada para apoyar experimentos en tierra que buscan los modos B de la polarización del fondo cósmico de microondas (CMB, por sus siglas en inglés). CalSat emitirá una serie de señales polarizadas conocidas para calibrar experimentos en busca de dichos modos B. Sin embargo, dada la debilidad de los mismos, estos experimentos necesitan procesos de calibración robustos para poder detectarlas. Las fuentes naturales utilizadas hoy en día para estas calibraciones no están bien caracterizadas lo que tiene un impacto directo en las incertidumbres de medición. La fuente de calibración propuesta en CalSat estará compuesta por tres frecuencias centrales, a 40, 90 y 150 GHz, que son frecuencias de interés en la búsqueda de los esperados modos B. CalSat mejorará la precisión instrumental, lo que facilitará la detección de los modos B de polarización, por ejemplo, reduciendo el error del ángulo polar al nivel del minuto de arco. Además, gracias a la estrategia de calibración propuesta, CalSat contará con una visibilidad óptima para experimentos en tierra ubicados en Atacama y Tenerife. Finalmente, nuestros resultados sobre el control térmico, determinan que CalSat no saturará ningún experimento estudiado debido a la emisión térmica.

Keywords: CMB polarization, Calibration, Micro-satellite, B-modes

1 Introduction

In this work we study the application of a calibration satellite (CalSat), which is designed to support ground-based experiments measuring the polarization signals in the Cosmic Microwave Background (CMB). It is now well established and accurately measured by several experiments (like the Wilkinson microwave anisotropy probe (WMAP), Page et al., 2006) that temperature anisotropies in CMB offer one of the best probes of early Universe, which could potentially lead to a precise determination of a large number of cosmological parameters (Jungman et al., 1996). Strong theoretical arguments suggest the presence of fluctuations in the polarized component of the CMB (so-called B-modes) at a level of 5-10% of the temperature anisotropy. According to the inflationary paradigm, which predicts an accelerated expansion of the Universe occurred at t $\approx 10^{-34}$ sec after the Big Bang, these anisotropies are the signature of a stochastic background of tensor perturbations (i.e. gravitational waves) that permeated the primordial Universe. These gravitational waves would have produced polarization signals separable from E-modes by their divergence-free 'B-mode' signature (Kamionkowski et al., 1997; Zaldarriaga and Seljak, 1997). However, the B-mode remains undetected, given that these polarization signals are orders of magnitude fainter than the temperature fluctuations and are obscured by the polarized Galactic foregrounds. A positive detection of B-modes in the CMB on the degree angular scales would provide us with important evidence in favor of the inflationary paradigm. In particular, it would allow us to constrain the value of the tensor-to-scalar ratio r, which is commonly parameterized as the signal amplitude of the inflationary gravitational wave (IGW). In other words, this parameter express the ratio between the amplitudes of tensor and scalar modes, and is related to the energy scale of inflation (Baumann et al., 2009). Currently, the tightest constraint on the amplitude of the gravitational waves parameterized through the tensor-to-scalar ratio $r < 0.036$ comes from combining the Planck and WMAP data with the BICEP/Keck measurement of the recombination peak (Ade et al., 2021). In addition to the IGW signal, other CMB polarization signals promise to deliver valuable cosmological information. Non-primordial B-modes are generated when E-modes are gravitationally lensed by large-scale structures in the universe.

Multi-frequency observations are required to disentangle the very weak CMB signal from diffuse polarized foregrounds originating by radiative processes in our galaxy. At frequencies lower than 100 GHz, the polarized sky emission is dominated by synchrotron radiation from electrons moving in the galactic magnetic field. Above that frequency, thermal emission from the interstellar dust is the major contaminant.

Instruments in satellites supported by sensitive ground-based experiments are in conditions to measure the B-mode signal over the full (or partial) sky. However, due to the signal weakness, the instruments must be subject to precise calibration processes. For the case of ground-based experiments, this could be achieved using a CalSat with a low Earth orbit (LEO) and emitting a purely polarized microwave signal (Nati et al., 2017; Johnson et al., 2015). As a result, the observations will benefit, from the absolute calibration of the polarization angle and the detectors beam response, meeting the accuracy requirements for the next generation of CMB experiments.
In section 2 are described the mechanisms which induced systematics errors and how to mitigate them. Section 3 describes the main features of ground-based experiments that CalSat could incise. In section 4 are described the types of artificial calibration satellites that can be proposed nowadays, as the types of calibration signals and the proposed calibration strategy.

Section 5 shows the calculus of the spurious received power due to the thermal emission of CalSat. Finally, in section 6 are presented some conclusions.

2 Polarimeter Calibration

Current and future CMB polarization experiments are aiming at an unprecedented level of sensitivity, therefore systematic effects that until today were less important than statistical uncertainties are becoming the most significant limitation. In this work we are going to focus in the polarization angle calibration aspects. An apparent polarization rotation produces a power leakage from E-mode spectrum into B-mode signal that results in a systematic signal in the B-modes spectrum and in the TB and EB cross spectra encoding the correlation of temperature (T) and E-mode signals with B-modes. The magnitude of the forecasted TB, EB and B-mode signals is faint when compared with instrument induced systematic errors. Therefore, the experiments trying to measure these signals need a robust polarimeter calibration program that will allow to mitigate the effect of these instrument induced errors during data analysis.

The instrument-induced polarization rotation (IPR), which is one of the most critical systematic errors, it still does not have a robustly established mitigation strategy. This instrumental effect rotates the apparent orientation of the linearly-polarized pseudo-vectors on the sky, and this rotation converts the brighter E-modes into spurious B-modes. Calibration of the detector's pixel rotation is one of the most challenging tasks facing the instrumentalists. A miscalibration of the detector's polarization angle by an amount $\Delta\psi$ rotates primordial Stokes parameters $\tilde{Q}(p)$, and $\tilde{U}(p)$ into the observed quantities:

$$Q(\boldsymbol{p}) \pm iU(\boldsymbol{p}) = e^{\pm 2i\Delta\psi}(\tilde{Q}(\boldsymbol{p}) \pm i\tilde{U}(\boldsymbol{p})) \tag{1}$$

The measured Fourier modes, $E(\boldsymbol{I})$ and $B(\boldsymbol{I})$, written in terms of the primordial modes $\tilde{E}(\boldsymbol{I})$ and $\tilde{B}(\boldsymbol{I})$, become

$$\begin{aligned} E(\boldsymbol{I}) &= \cos(2\Delta\psi)\tilde{E}(\boldsymbol{I}) + \sin(2\Delta\psi)\tilde{B}(\boldsymbol{I}) \\ B(\boldsymbol{I}) &= -\sin(2\Delta\psi)\tilde{E}(\boldsymbol{I}) + \cos(2\Delta\psi)\tilde{B}(\boldsymbol{I}) \end{aligned} \tag{2}$$

The above equations show that pixel rotation modifies the power spectra of $E(l)$ and $B(l)$ and generate spurious correlation between $E(l)$ and $B(l)$ and between $T(l)$ and $B(l)$, modifying the observed power spectra as follows (Koopman et al., 2016),

$$\begin{aligned} C_\ell^{TE} &= \cos(2\Delta\psi)\tilde{C}_\ell^{TE} \\ C_\ell^{EE} &= \sin^2(2\Delta\psi)\tilde{C}_\ell^{BB} + \cos^2(2\Delta\psi)\tilde{C}_\ell^{EE} \\ C_\ell^{EB} &= \frac{1}{2}\sin(4\Delta\psi)(\tilde{C}_\ell^{BB} - \tilde{C}_\ell^{EE}) \\ C_\ell^{TB} &= -\sin(2\Delta\psi)\tilde{C}_\ell^{TE} \\ C_\ell^{BB} &= \cos^2(2\Delta\psi)\tilde{C}_\ell^{BB} + \sin^2(2\Delta\psi)\tilde{C}_\ell^{EE} \end{aligned} \tag{3}$$

The tildes represent primordial quantities. From Equation 3 it is clear that pixel rotation generates spurious B-modes in the absence of primordial B-modes. As a result, current constraints on $\Delta\psi$ are limited by the systematic error associated with calibrating the polarization angle of the detectors. Calibration of the pixel rotation involves finding $\Delta\psi$ for the detector

system and removing it from the data. This procedure will recover the unrotated, primordial CMB polarization spectra.
To calibrate the intensity of the CMB, sky signals from known sources are commonly used. Nevertheless, there is no a good known source for calibrating experiments aiming to detect B-mode polarized signal, given that, these sources should be well characterised and have purely polarized signals. There are some astronomical objects (for instance, Tau-A) which could works as calibration sources, however, since that these are not point-like sources, are frequency dependent, and have time variability, they do not accomplish the requirements to be an ideal calibrator as the systematic required. To properly characterize the IPR properties of a CMB polarimeter, a linearly polarized source with known polarization properties should be observed with high precision. The ideal source should be point-like and generate a high signal-to-noise signal with an integration time of a few seconds. Also, this signal should not be too bright (a power less than a few pW, as is discussed in Section 5) since this could saturate the detectors.

In order to quest an IGW signal with a tensor-to-scalar ratio of $r > 0.01$, the orientation of the polarization of the observed source on the sky must be known to 0.2° or better (Bock et al., 2006). Among the partially polarized astrophysical sources, at milimeter wavelengths, the Crab Nebula, or Tau A is the best option. This is an extended polarized supernova remnant with an angular extension of $7' \times 5'$. Among other characteristics, Tau A it is not too bright enough to give a high-to-noise signal ratio measurement with a short integration time, this source allows an accuracy for the polarization orientation between 1° and 0.5° (Aumont et al., 2020). Therefore, though Tau A is the best polarized source on the sky at millimeter wavelengths, it does not meet the performance requirements of a calibrator for an IGW-signal search.
The standard cosmological model predicts that TB and EB identically vanish, which means that the odd-parity signal (B) should be completely unrelated to intensity (T) and even-parity signals (E) in the early Universe. Taking into account this relation many current experiments 'self-calibrate' their polarization angles (Bigot-Sazy et al., 2013; Keating et al., 2012), at the expense of losing detection capability on genuine physical quantities. This initial assumption is not true in the presence of phenomena that produce non-vanishing TB and EB. In addition, this method destroys the possibility to measure or to place limits on phenomena that generate TB and EB spectra, like Cosmic Birefringence, Faraday Rotation and chiral gravity models.

The POLarization Orientation CALibrator for Cosmology, POLOCALC, presented a method to measure the absolute orientation of the polarization plane of the CMB photons with an accuracy of between 0.01° and 0.001° (Nati et al., 2017). This was proposed to dramatically improve instrumental accuracy by means of an artificial calibration source flying on high-altitude balloons and aerial drones. A balloon-borne calibrator would provide a source in the far field of larger telescopes, while an aerial drone can be used for tests and smaller polarimeters. The source would make use of both narrow and broad-band microwave emitters between 40 and 150 GHz coupled to precise polarizing filters.

In Fig.1 it is show the BB mode power spectra of the spurious signals produced by systematic errors produced by polarization rotation. Blue curves represent the spurious signal produced by 30, 10, 3 and 1 arc-min (0.5, 0.17, 0.05, and 0.017 degrees) of polarization rotation (Casas-Reinares et al., 2021). Primordial B-mode (solid black lines), gravitational lensing B-mode (dashed black) and the EE (solid green) signals are also plotted for reference.

As we already know, 30 arc-min is approximately the current error level set by the systematic uncertainty in available calibration sources. A miscalibration of 0.5° in the polarization orientation translates into a spurious B-mode signal corresponding to a tensor-to-scalar ratio of $r \sim 0.01$ (Abitbol et al., 2016), affecting the sensitivity range of existing and planned experiments.

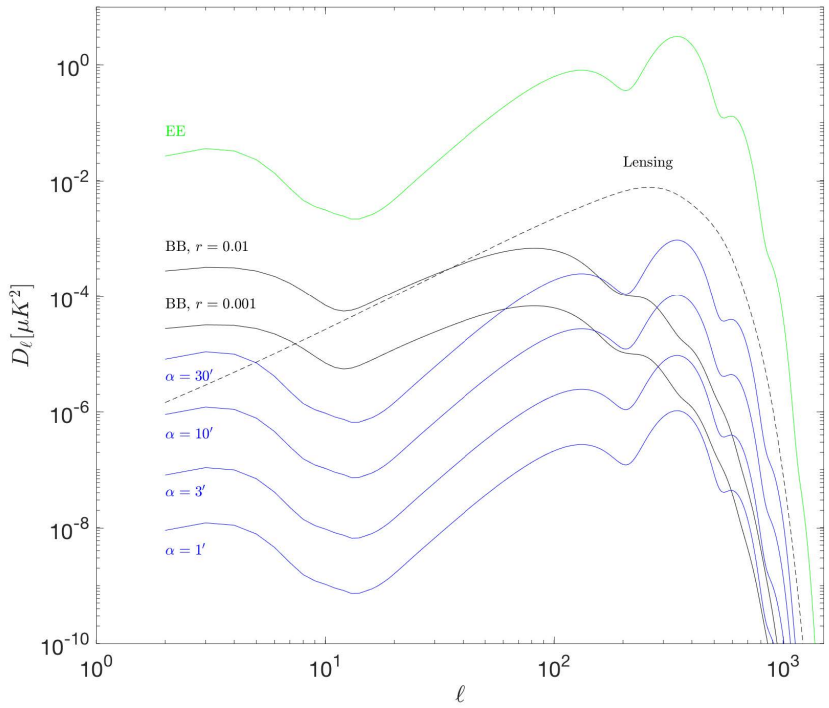

Figure 1: *Systematic errors in the BB angular power spectra per logarithmic interval produced by polarization rotation. The spurious signal produced by 30, 10, 3 and 1 arc-minutes of rotation are represented by the blue curves. Primordial B-mode for two values of r (solid black lines), gravitational lensing B-mode (dashed black) and the EE (solid green) spectra are plotted for reference. From Casas-Reinares et al., 2021.*

The calibration sources of a CalSat would allow the reduction of any polar angle error below the 1 arc-minute blue curve. This suppressed error level is negligible for current experiments targeting $r \approx 0.01$ and future experiments (like The CMB-S4 Collaboration et al., 2016 and LiteBIRD mission (Lee et al., 2019)) that will target $r \approx 0.001$.

3 Ground-based experiments

We shall focus in experiments located in the Atacama desert in Chile as: the Cosmology Large Angular Scale Surveyor (CLASS); (Harrington et al., 2016), the Q&U Bolometric Interferometer for Cosmology (QUBIC); (Mele et al., 2020) , and the Advanced Atacama Cosmology

Telescope (AdvACT); (Thornton et al., 2016), and experiments located in Tenerife island in Spain as: QUIJOTE (Q-U-I JOint TEnerife); (Poidevin et al., 2018) and the Large Scale Polarization Explorer (LSPE)-STRIP; (Addamo et al., 2021). Given the location, sensitivity and the frequency bands at which these telescopes operate, these are fundamental in the quest for the B modes. In the following scientific goals and instrumentation characteristics of each experiment will be provided to have an idea of the calibration needs that are required.

3.1 Atacama experiments

The CLASS experiment is a four telescope array designed to characterize relic primordial gravitational waves from inflation at angular scales ($2 < \ell \lesssim 200$), with the aim of measuring a primordial B-mode signal at a sensitivity level of r ≈ 0.01 (95% C.L.), and the optical depth to reionization through a measurement of the polarized CMB. CLASS is uniquely designed to measure the primordial B-mode signal from both reionization and recombination over a frequency range straddling the foreground minimum (see Fig. 2). This experiment is operating from a high-altitude site in the Atacama Desert in Chile (22° 58' S, 67° 47' W) and will survey 70% of the sky in four frequency bands centred at 40 (Q-band), 90 (W-band), and 150/220 (dichroic G-band) GHz. Telescopes operating at 90 GHz are optimized for CMB observation near the minimum in the polarized Galactic emission, a 40 GHz telescope probes polarized synchrotron emission, and a 140/220 GHz telescope probes polarized dust. Each CLASS telescope counts with a 200 sq-deg field-of-view (FOV) enable recovery of CMB polarization at angular scales $\gtrsim 2°$, and each telescope counts with a 46 cm vacuum-window aperture (Harrington et al., 2016).

The Fig. 3 shows progress and forecasts for the CLASS B-mode measurement. The plot shows that SPT, Polarbear, and BICEP2/Keck have detected B-mode polarization due to gravitational lensing of E-mode polarization. The measurements at $\ell \sim 100$, the "recombination peak", are susceptible to the lensing foreground whereas this contamination is negligible for the "reionization peak" at $\ell < 10$. The CLASS sensitivity per $\log(\ell)$ for $r = 0.01$ is shown in the plot by the red envelope, indicating sensitivity to both the recombination and reionization peaks. With the exception of CLASS, all on-going measurements are designed to focus on the recombination peak and thus do not reach the largest scales.
In Table 1 we can see an optical performance summary of the CLASS telescope. Due to its characteristics and scientific goals, polarization angle error lower than 0.2 degrees should be achieved by means of calibration.

Telescope	**Band [GHz]**	**Beam (FWHM) [arcmin]**	**No. of Optical Detectors**	**Detector Noise Temperature** $[\mu K_{cmb}\sqrt{s}]$	**Array Noise Temperature** $[\mu K_{cmb}\sqrt{s}]$
40 GHz [a]	33 - 43	90	70	180	22
90 GHz	77 - 108	40	319	346	19
150 GHz	127 -163	24	389	453	23
220 GHz	200 - 234	18	211	1034	71

Table 1: *Optical performance summary for CLASS telescopes.* [a] *40 GHz optical performance after April 2018 upgrade. The values in parentheses correspond to the telescope's performance with the TG filter installed. From Dahal et al., 2022.*

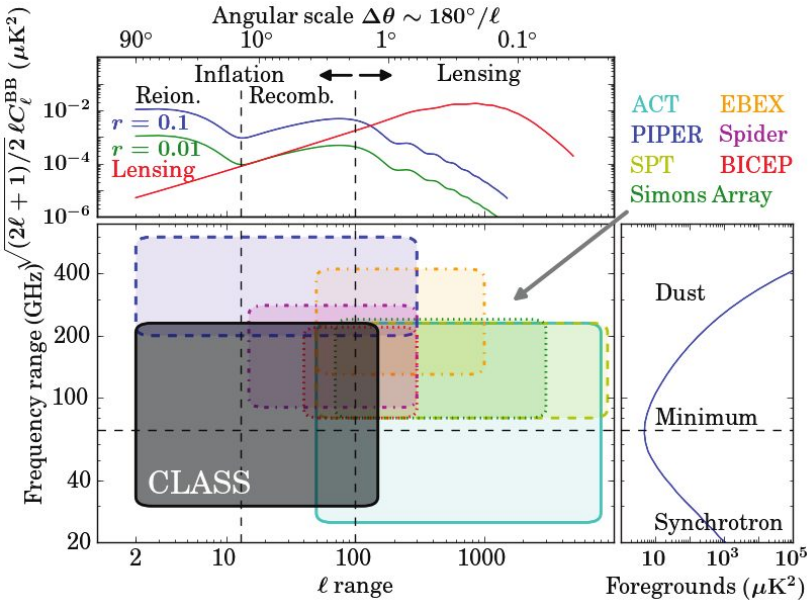

Figure 2: *The figure gives the multipole (ℓ) and frequency range of current surveys with forecasted constraints at the $r \sim 0.01$ level, similar to CLASS. Top and side plots show the B-mode angular power spectrum and the frequency spectrum of polarized dust emission and synchrotron radiation, (Harrington et al., 2016).*

The ACT is an off-axis Gregorian telescope with a six-meter aperture, constructed in 2007 in the Atacama Desert, located at 5190 m altitude in Chile (Fowler et al., 2007). Like CLASS, ACT uses transition edge sensor (TES) detector arrays to measure CMB temperature and polarization anisotropies at multiple frequencies. The Atacama Cosmology Telescope Polarimeter (ACTPol) is a polarization sensitive receiver upgrade to ACT, and measures the small angular scale polarization anisotropies in the CMB. The full focal plane is composed of three detector arrays, the first two detector arrays, observing at 146 GHz, and the third array observing at 90 and 146 GHz. The Advanced ACTPol (AdvACT) is the third-generation CMB telescope for the ACT project. The AdvACT experiment is an upgraded instrument for the ACT aims to improve the measurement of the cosmic microwave background anisotropies and polarization. This upgrade, approximately double the number of detectors, each with improved sensitivity, and add three more frequency channels compared to the previous ACTPol receiver (Henderson et al., 2016). This experiment counts with a total of five operating frequencies bands: 28/41 GHz, 90/150 GHz, and 150/230 GHz. Each set of optics has a field of view (FOV) that spans approximately 1° on the sky (Thornton et al., 2016). Polarization systematics is controlled with the use of ambient temperature continuously rotating half-wave plates (HWPs), which modulate the incoming polarized signals, helping in the control systematics.
Figure 4 shows the predicted errors on EE- and BB-mode power spectra expected for the AdvACT experiment, as compared with the spectra expected for different values of r and $\sum m_\nu$ (sum of the neutrino masses).

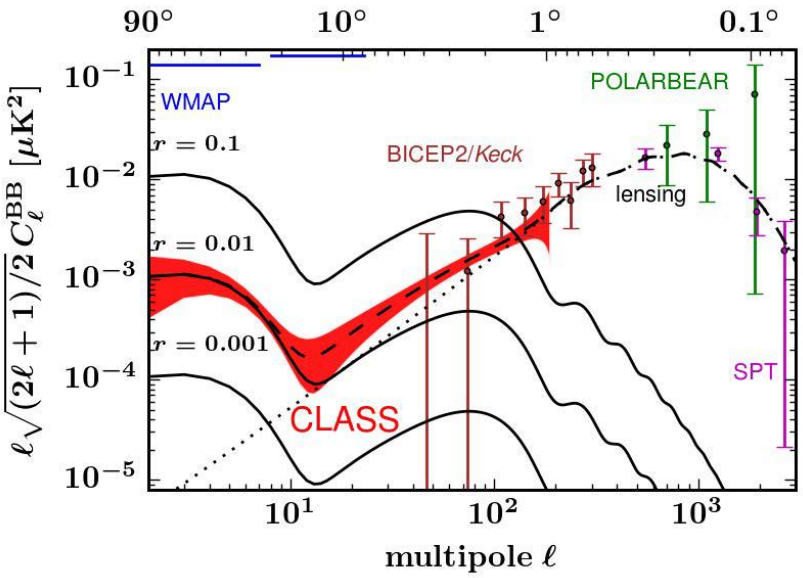

Figure 3: *The CLASS B-mode Measurement. The figure shows the power spectra for B-mode amplitudes of $r = 0.1$, 0.01, and 0.001 with peaks at multipole moments $\ell < 10$ (the 'reionization peak') and $\ell \approx 100$ (the 'recombination peak'). The dashed curve shows the lensing of E-modes. From Harrington et al., 2016.*

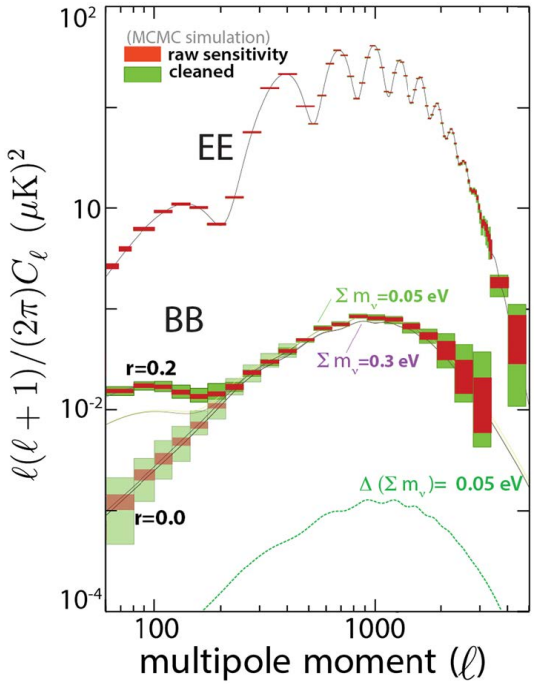

Figure 4: *Forecast AdvACT errors on EE and BB spectra, compared to ΛCMD predictions, for several values of r and $\sum m_\nu$. The red errors bars indicate the raw sensitivity. The green error bars indicate an estimate for the degradation due to cleaning foregrounds. From Henderson et al., 2016.*

The red boxes show projected errors on the power spectra based on the predicted AdvACT raw instrument sensitivity, while the green boxes show projections after using the wide spectral coverage of AdvACT in conjunction with Planck measurements at 353 GHz to remove dust foregrounds three times larger than in the Planck Sky Model (PSM), (Delabrouille, J. et al., 2013).
AdvACT deploy four new multichroic arrays, as summarized in Table 2.

Detector array	**Center freq. (GHz)**	**Width (GHz)**	**# TES**
LF	28	6	88
LF	41	19	88
MF	90	39	1712
MF/HF	150	41	2718
HF	230	100	1006

Table 2: *AdvACT deploy four multichroic arrays; a high-frequency (HF) array operating at 150 and 230 GHz, two medium frequency (MF) arrays operating at 90 and 150 GHz, and a low-frequency (LF) array operating at 28 and 41 GHz.*

Due to its characteristics and scientific goals, polarization angle error lower than 0.1 degrees should be achieved by means of calibration.

The Q & U Bolometric Interferometer for Cosmology (QUBIC) is a novel ground-based experiment also dedicated to the measurement of the B-mode polarization of the CMB. QUBIC is designed with a novel approach that combines the advantages of interferometry in terms of control of instrumental systematic effects with those of bolometric detectors in terms of wide-band, background-limited sensitivity. Due to this, in the following, a more detailed description than in the previous experiments is provided. The QUBIC synthesized beam has a frequency-dependent shape that results in the ability to produce maps of the CMB polarization in multiple subbands within the two physical bands of the instrument. It will observe at 150 GHz, and sample the range of multipoles $\ell \approx 30 - 200$ in the sky. A 220-GHz band will be added to improve astrophysical foreground subtraction. These features make QUBIC complementary to other instruments and makes it particularly well suited to characterize and remove Galactic foreground contamination. QUBIC will be installed near Atacama desert, in Argentina, near the city of San Antonio de los Cobres, at the Alto Chorrillos site, Salta Province. Its main parameters are summarized in Table 3.
QUBIC operates as a Fizeau interferometer; the sky radiation is collected from an array of back-to-back feedhorns at the entrance aperture of the instrument and their exit beams are combined. The signal from the sky enters through a window and series of filters and is modulated by a rotating half-wave plate (HWP). The HWP can be stepped between 7 positions, separated by 15°, ranging from 0° to 90°, to a precision of $< 0.2°$ at cryogenic temperatures. We can write the signal in terms of the electric field in orthogonal directions, then the signal after pass by the HWP will be (O'Sullivan et al., 2022),

$$S_{HWP} = \begin{pmatrix} E_x \cos 2\phi(t) + E_y \sin 2\phi(t) \\ E_x \sin 2\phi(t) - E_y \cos 2\phi(t) \end{pmatrix} \tag{4}$$

Parameter	Full Instrument value
Frequency channels	150 GHz & 220 GHz
Frequency range 150 GHz	[131-169] GHz
Frequency range 220 GHz	[192.5-247.5] GHz
Number of horns	400
Window Aperture [m]	0.56
Sky Coverage	1.5%
FWHM [degrees]	0.39 (150 GHz), 0.27 (220 GHz)
r upper-limit (68% C.L., no FG)	0.021 (150 GHz), 0.023 (220 GHz), 0.015 (Combined)

Table 3: *QUBIC main parameters. From Hamilton et al., 2022.*

where $\phi(t)$ is the time-varying angle of rotation of the HWP. A polarizing grid then removes the signal in one direction giving

$$S_{HWP} = \begin{pmatrix} E_x \cos 2\phi(t) + E_y \sin 2\phi(t) \\ 0 \end{pmatrix} \tag{5}$$

Also, we can write it in terms of the Stokes parameters, $S = I + Q\cos 4\phi(t) + U \sin 4\phi(t)$. This signal is convolved with the synthesized beam of the instrument. The modulation of the signal as a function of HWP angle $\phi(t)$ allows I, Q, and U to be reconstructed. A dichroic filter is used to split the signal into two frequency bands that can then be imaged simultaneously on orthogonal focal planes (as is show in Fig. 5). A sectional cut of the cryostat is show in Fig 5. The sky signal enters the cryostat through (1) a 56 cm diameter window. After the window there is (2) a series of thermal cutting of frequencies higher than the desired ones. The polarization of the incoming signal is modulated by (3) a rotating HWP before a single polarization is selected by (4) the polarizer. The signal is collected and then re-emitted into the combiner by (5) a circular array of 400 back-to-back corrugated feedhorns. The backhorns directly illuminate the two-mirrors (6 & 8) off-axis Gregorian optical combiner that focuses the signal onto the two perpendicular focal planes, separated by a dichroic filter (9) that splits the incoming waves into two wide bands centered at 150 GHz for the on-axis focal plane and 220 GHz for the off-axis one. (7) A cold stop is inserted between the primary and secondary mirrors to minimize stray light, (see O'Sullivan et al., 2022 for more details).

QUBIC scans the sky with a synthesized beam formed by the feedhorn array, that exhibits multiple peaks. A cut of the QUBIC synthesized beam is shown in Fig. 6 for the frequencies of 140 & 160 GHz. As the respective distance between peaks changes with frequency, the signal detected with a given bolometer will combine (through convolution with the synthesized beam) different directions on the sky for different incoming frequencies within the physical wide band. The field-of-view of the instrument, determined by the FWHM of the sky-facing horns, is 12.9° at 150 GHz, with secondary lobes below -25 dB (O'Sullivan et al., 2022).

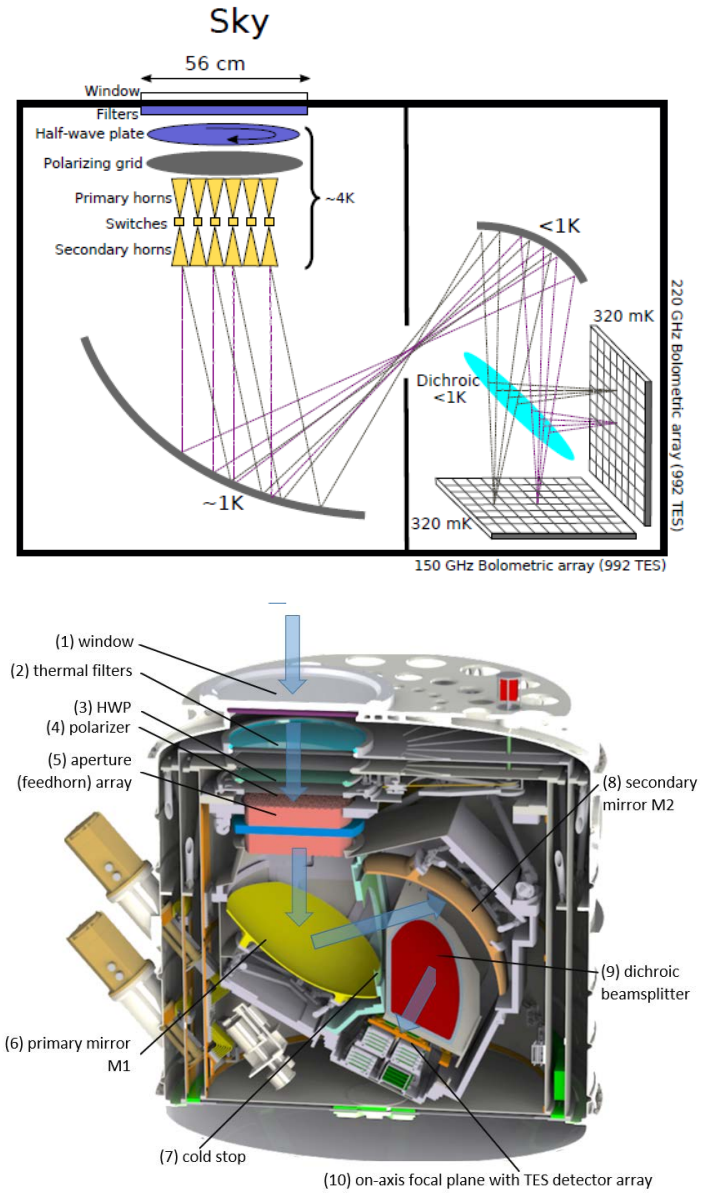

Figure 5: *Schematic of the QUBIC instrument (top) and sectional cut of the cryostat (bottom) showing the same sub-systems in their real configuration. From O'Sullivan et al., 2022.*

Measurements of the QUBIC Technological Demonstrator (TD) (64 back-to-back horns and mirrors reduced, 248 TES bolometer array operating at 150 GHz) cross polarization have made by Hamilton et al., 2022, they have found a median measured cross-polarization of 0.12% among the detectors and a 0.61% median 95% upper-limit. 77% of the detectors have a measured cross-polarization compatible with zero at the one-sigma level. Such low cross-polarization is an important feature for detecting a signal as small as the primordial B-modes. Further, Monte-Carlo simulations made in Hamilton et al., 2022, show that QUBIC has the statistical power (without foregrounds, atmospheric fluctuations and systematics) to constrain the B-modes down to a tensor-to-scalar ratio $r < 0.015$ at 68% C.L. ($r < 0.03$ at 95%

C.L.) with three years integration on the sky. In the presence of foregrounds, the numbers above are to be understood as our statistical sensitivity to effective B-modes including the contribution from primordial tensors as well as dust polarization.

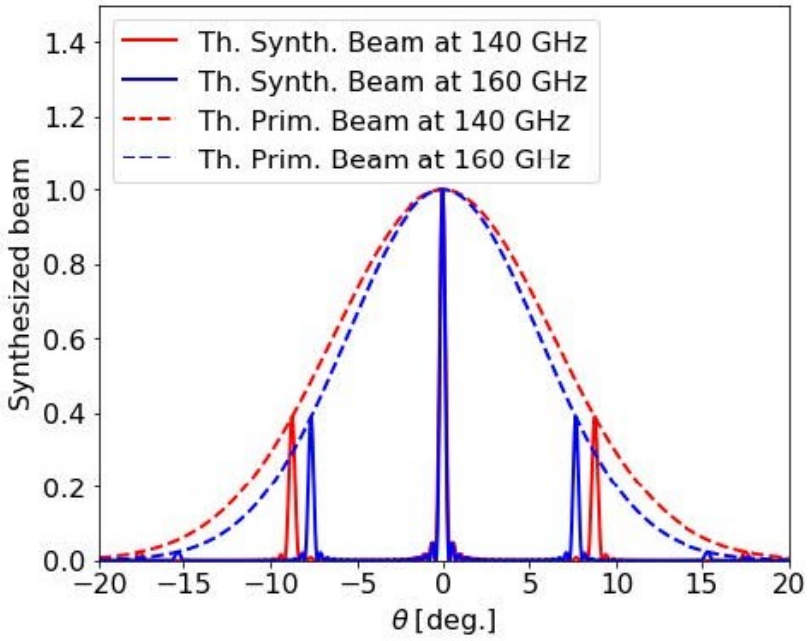

Figure 6: *A cut of the QUBIC theoretical synthesized and primary beams at two different frequencies for a bolometer located at the center of the focal plane. The figure shows how the location of the multiple peaks significantly changes for a small frequency change. This behaviour is at the basis of the spectral imaging capabilities offered by bolometric interferometry. From Hamilton et al., 2022.*

As in the previous experiments, the characteristics and scientific goals of QUBIC, require polarization angle error lower than 0.2 degrees, and noise floor of at least -60 dBi for optical beam characterization (O'Sullivan et al., 2022).

3.2 Tenerife experiments

QUIJOTE (Q-U-I JOint TEnerife) is an experiment installed in Teneide Observatory in the Canary Islands, Spain. It is located at an altitude of 2400 meters over the sea level at longitude, latitude position 28.3°N, 16.5°W (Rubiño-Martín et al., 2010). QUIJOTE is designed to detect a primordial gravitational-wave component if the B-mode amplitude is larger than $r = 0.05$. It consists of two telescopes (as is show in Fig. 7) based on an altazimuth mount supporting a primary (parabolic) and a secondary (hyperbolic) mirror disposed in an offset Gregorian Dracon scheme, which provides optimal cross polarisation properties (designed to be $\leq$ -35 dB) and symmetric beams. QUIJOTE have three linear polarimetry instruments covering respectively the frequencies 10-20, 31 and 42 GHz with an angular resolution of ~ 1 degree.

The multi-frequency instrument (MFI) is a multi-channel instrument with four independent sky pixels: two operate at 10-14 GHz, the other two at 16-20 GHz. The instrument was initially designed with five chains of polarimeters although the central one, corresponding to the frequency of 30 GHz was not mounted. The MFI is dedicated primarily to the characterization of the polarized foregrounds. The MFI polarimeters design is shown in the schematic diagram in Fig. 8 (top). Each polarimeter consists of a partially cooled feedhorn, a cooled-rotating polar modulator, a cooled orthomode transducer (OMT), two cooled Low Noise Amplifiers (LNAs) and a Back End Module (BEM). The two outputs from the cold Front-End (FE) are fed into phase adjusters, further amplification and band pass filters before being split into two signals. All the the polarimeters have simultaneous Q and U detection; i.e the two orthogonal polar signals are also correlated through a 180° hybrid and passed through two additional detectors. Rotation of the polar modulator causes the outputs to be interchanged between Q and U. Sufficiently rapid rotation of the polar modulator allows a complete removal of 1/f noise from the measurement of Q and U for all the MFI frequencies. This also allows complete independent Q, U and I measurement for each of the 4 outputs. The data obtained from the QT1 with the MFI show a high symmetric beam with ellipticity > 0.98 with very low far sidelobes (≤-40dB) and polarization leakage (≤-25dB) (Poidevin et al., 2018).

The TGI and the FGI instruments were initially focused on B-mode science. TGI is filled with 30 polarimeters working in the range of 26-36 GHz. Each pixel presents 4 output signals providing data to the acquisition system. The polarization modulation is obtained by combining two phase-switches, each of them having four different possible phase states, i.e. 0°/90°/180°/270°. After laboratory tests, it has been shown that the spinning polar modulators in a cryogenic environment is not appropriate for the long-term operations required for the TGI. Thus, the receiver configuration was modified by replacing the rotating polar modulator with a fixed polarizer. The current design is shown in Fig. 8 (bottom). It includes a fixed polariser and phase switches to generate four polarisation states to minimize the different systematics in the receiver. The FGI instrument incorporate 30 polarimeters at 40 GHz. The conceptual design of the polarimeter chain is identical to the TGI.

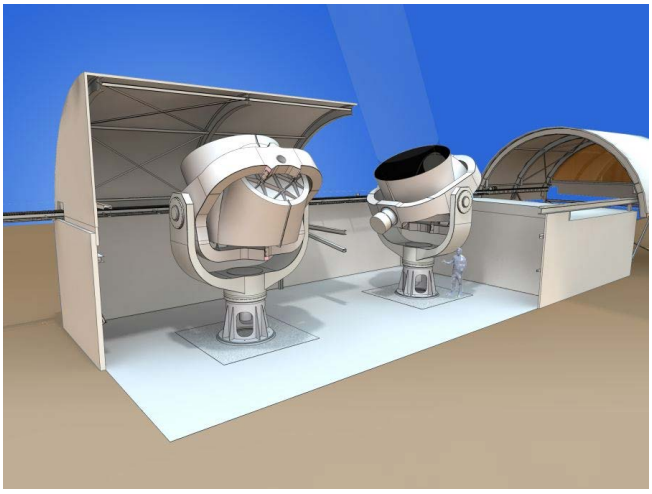

Figure 7: *3D drawing of the QUIJOTE-CMB experiment dome and the two telescopes. Each primary mirror has a 2.25 m projected aperture. From Rubiño-Martín et al., 2012.*

The MFI maps will be used to correct the high frequency channels of QUIJOTE to search for the primordial B-modes. The Fig. 9 shows the scientific goal, it shows the angular power spectrum of the E and B modes after 3-year of effective observing time, assuming a sky coverage of 5,000 square degrees. The two instruments (FGI and TGI) can be operated simultaneously, one in each telescope. The Fig. 9 correspond to the optimal situation in which the foreground removal leaves a negligible impact on the power spectrum.

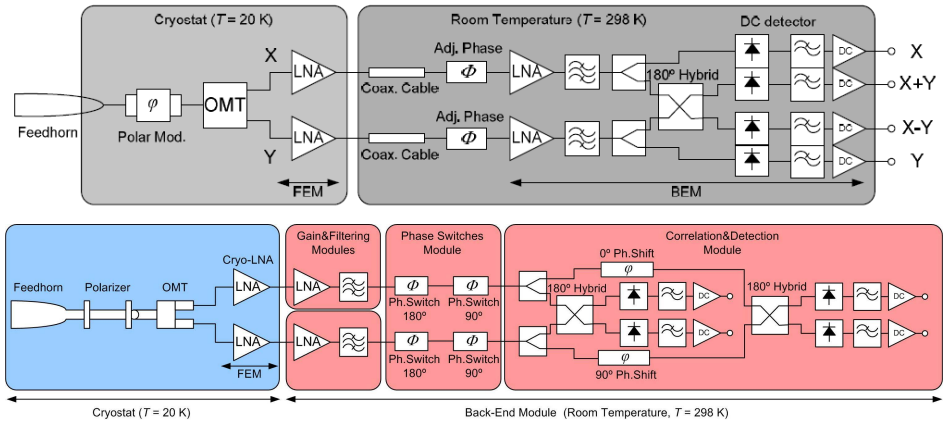

Figure 8: *(top) A schematic diagram of the MFI polarimeter configuration. (bottom) Configuration of each of the 31 receivers of the TGI. From Hoyland et al., 2012 and Rubiño-Martín et al., 2010.*

The Table 4 summarizes the basic (nominal) characteristic of these three instruments in QUIJOTE.

	MFI				TGI	FGI
Nominal Frequency [GHz]	11	13	17	19	30	40
Bandwidth [GHz]	2	2	2	2	8	10
Number of horns	2	2	2	2	31	40
Channels per horn	4	4	4	2	4	4
Beam FWHM [°]	0.92	0.92	0.60	0.60	0.37	0.28
T_{sys} **[K]**	25	25	25	25	35	45

Table 4: *Nominal characteristics of the three QUIJOTE-CMB instruments: MFI, TGI and FGI. Tsys stands for the total system temperature. From Rubiño-Martín et al., 2012.*

Due to the characteristics and scientific goals of QUIJOTE, polarization angle error lower than 0.5 degrees should be achieved by means of calibration.

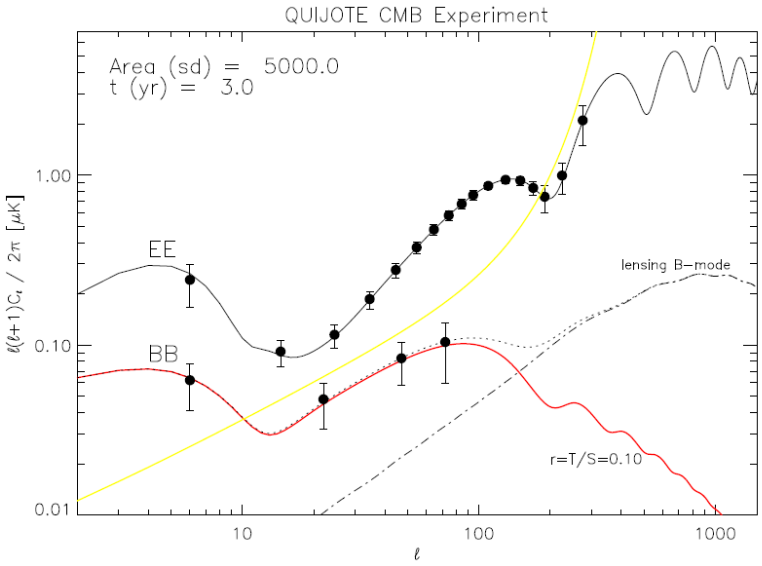

Figure 9: *QUIJOTE scientific goal for the angular power spectrum of the CMB E and B mode signals. It is shown the case for 3 years operation time, and a sky coverage of ~ 5,000 square degrees. The red line corresponds to the primordial B-mode contribution in the case of r = 0.1. Yellow line indicates the associated QUIJOTE noise power spectrum. Dots with error bars correspond to averaged measurements over a certain multipole band. From Rubiño-Martín et al., 2010.*

The Large Scale Polarization Explorer (LSPE) is a cosmology program for the measurement of large scale curl–like features (B–modes) in the polarization of the CMB. LSPE counts with two instruments which work synergically by covering a large portion of the northern microwave sky. LSPE/STRIP is a coherent array of receivers planned to be operated from the Teide Observatory in Tenerife. The main objective of this instrument is the characterization of the low–frequency polarized signals of galactic origin; LSPE/SWIPE is a balloon–borne bolometric polarimeter based on 330 large throughput multi–moded detectors, designed to measure the CMB polarization at 150 GHz and to monitor the polarized emission by galactic dust above 200 GHz.
One of the main scientific target is the detection of B-mode of CMB polarization at a level corresponding to a tensor-to-scalar ratio r = 0.03 with 99.7% confidence level (C.L.); or an upper limit to tensor-to-scalar ratio r = 0.015 at 95% C.L. (Addamo et al., 2021). Table 5 reports the basic parameters for the two instruments, in the baseline configuration.
We focus in LSPE-Strip given that our work if focused in ground-based experiments. LSPE-Strip is a coherent polarimeter that will observe the sky in two frequency bans centred at 43 GHz (Q-band, 49 polarimeters) and 95 GHz (W-band, 6 polarimeters) through a dual-reflector crossed-Dragone telescope of ~ 1.5 m projected aperture. The telescope provides an angular resolution of ~ 20′ in the Q-band and ~ 10′ in the W-band.

Instrument	**Strip**		**SWIPE**		
Site	Tenerife		ballon		
Frequency [GHz]	43	93	145	210	240
Bandwidth	17%	8%	30%	20%	10%
Angular resolution FWHM	20'	10'		85'	
Field of view	5°			11°	
Number of polarimeters (Strip) Detectors (SWIPE)	49	6	162	82	82
NET ($\mu K_{CMB}\sqrt{s}$)	515	1139	12.6	15.6	31.4
Observation time	2 years		8 - 15 days		

Table 5: *LSPE baseline instrumental parameters. From Lamagna et al., 2020.*

Addamo et al., 2021 have simulated the main beam radiation patterns using the Physical Optics (PO) method. Given the off-axis configuration, the main beams are characterized by several parameters, such as the angular resolution, the ellipticity, the main beam directivity, and the cross-polar discrimination factor (XPD). On the other hand, the sidelobes have been computed using Multi-Reflector Geometrical Theory of Diffraction (MrGTD). Each contribution has been analyzed separately and then combined in an integrated model beam. Addamo et al., 2021 find that the level of sidelobes at angles larger than 1° is less than -55 dB at 43 GHz and less than -65 dB at 95 GHz.

In the left panel of Fig. 10 it is show the footprint of the Strip main beams in the $(u; v)$ plane. We can see the 49 Q-band beams grouped in seven hexagonal structures of seven beams each and the six outer W-band beams. In the right panel it is shown a cut corresponding to $\phi = 0$ of the central beam. The beam section for $\theta < 0$ has been flipped on the positive axis to better highlight the asymmetries.

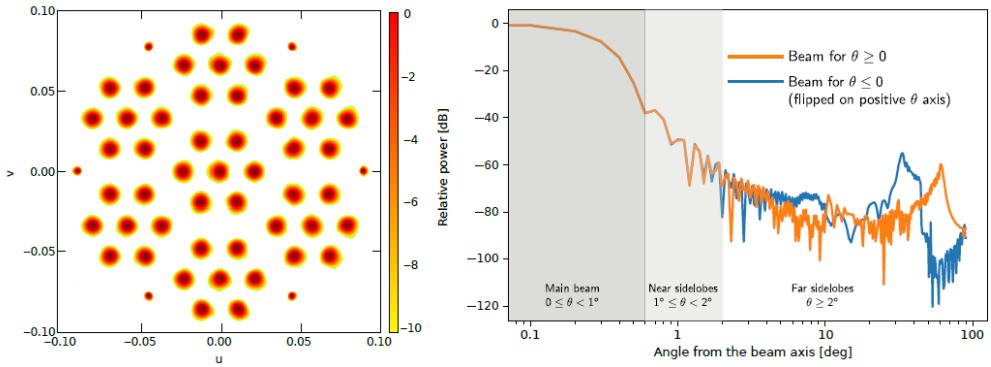

Figure 10: *Left: footprint of the LSPE-Strip main beams in the (u; v) plane (large beams, 43 GHz, small beams, 95 GHz). Right: beam cut for $\phi = 0$ of the central horn. The (u; v) variables are defined as $u = \sin(\theta)\cos(\phi)$, $v = \sin(\theta)\sin(\phi)$, where $(\theta; \phi)$ are standard spherical coordinates, with the center of the telescope pointing towards $\theta = 0$. From Addamo et al., 2021.*

The design of the STRIP polarimeters is based on Indium Phosphide (InP) cryogenic

High Electron Mobility Transistor (HEMT) low noise amplifiers integrated in Monolithic Microwave Integrated Circuits (MMIC) and on high–performance waveguide components cooled to 20 K. A schematic of the detection chain of STRIP is shown in Fig. 11. The correlation unit receives the circular polarization coming from the orthomode transducer; each input is amplified and phase modulated by phase shifters. One phase switch shifts the phase between 0° and 180° at 4 kHz, while the other works at 100 Hz. These signals propagate through a symmetric 180° hybrid, the power detected at its output is a combination of I and Q Stokes parameters, with Q having opposite signs at the two detectors. The detected power at the output of a second, 90° hybrid coupler yields a combination of I and U, with U appearing with opposite signs. The design takes full advantage of the coherent nature of the signal, implementing a double demodulation scheme to minimize residual systematic effects. This strategy allows Strip to recover both Q and U from a single measurement, after combining the two linearly polarized components of the input field, E_x and E_y, into left and right circular polarization components.
The characteristics and scientific goals of LSPE, require polarization angle error lower than 0.1 degrees, and noise floor of at least -70 dBi for optical beam characterization.

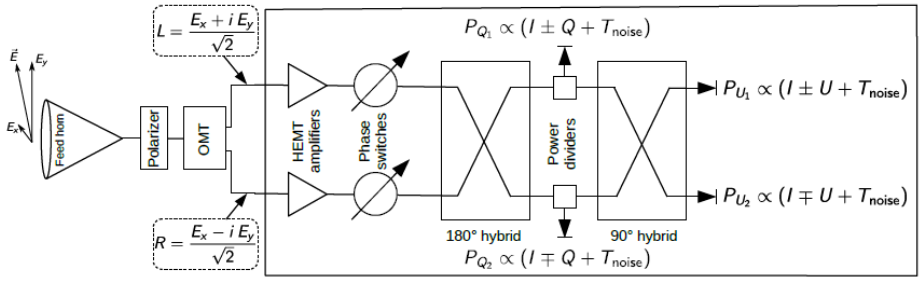

Figure 11: *The Strip polarimeter operation principle. The figure also shows the main mathematical relationships among the detected power at the four diodes, $P_{Q_{1,2}}$; $P_{U_{1,2}}$, the Stokes parameters defined in the polarizer reference frame, I, Q, U and the polarimeter noise temperature, T_{noise}. From Addamo et al., 2021.*

4 CalSat description

In this work is proposed the use of a calibration source that is expected to be embarked in the upcoming UPM-Sat 3 micro-satellite, which would be flying in a sun synchronous orbit (SSO). The proposed calibration system is expected to cover the needs of both, small and large aperture experiments. For small apertures experiments (CLASS, QUBIC), and for large apertures (QUIJOTE, LSPE-STRIP, ACT), this calibration system will allow, between others, the calibration of the polarization angle, far field measurements of the telescope beam patterns, and the calibration of the intensity response. From CalSat a set of microwave sources will emit linearly polarized signals at different wavelengths, covering, at least partially, the frequency bands of the ground-based experiments.

4.1 Types of calibration satellites

In order to accomplish the calibration requirements of the experiments detecting B-modes signals in the CMB, different types of artificial calibration sources have been proposed. Some of the main calibration instruments to be implemented in ongoing and future CMB polarization experiments are described here.
In Johnson et al., 2015 it is described a CubeSat-based calibration instrument called CalSat that is designed to support ground-based and suborbital experiments searching for various polarization signals in the CMB. CubeSats are cube shaped picosatellites with dimensions and features outlined in the CubeSat Specification Drawing (see Appendix B in Johnstone, 2020). The Poly Picosatellite Orbital Deployer (P-POD) defines a CubeSat standard, and Cubesats must conform to a strict list of requirements so that they are compatible with the P-POD. Among these requirements is a volume requirement. The fundamental CubeSat size is 10 cm × 10 cm × 10 cm and this size is referred to as '1U', but larger 2U (10 cm × 10 cm × 20 cm) and 3U (10 cm × 10 cm × 30 cm) sizes also can fit into the P-POD (Johnstone, 2020). CalSat is based on a 3U CubeSat and the primary CalSat characteristics are summarized in Table 6.

Characteristic	**Value**
Source frequencies [GHz]	47.1, 80.0, 140, 249 and 309
Source spectral width [MHz]	<1
Polarization	Linear
Cross-polarization level [dB]	-60
Horn type	Conical
Polarization orientation uncertainty [°]	0.05
Orbit altitude [km]	500
Ortibal period [hours]	1.6
Orbits per day	15.2

Table 6: CalSat characteristics. From Johnson et al., 2015.

In Casas-Reinares et al., 2021 is also described a calibration satellite called L2-CalSat based on a 6U CubeSat. The main payload of L2-CalSat is a multi-frequency variable source. In the proposed calibration system a set of microwave sources will emit linearly polarized signals at different wavelengths. Focusing in a frequency band from about 40 to 400 GHz, it is proposed to cover six bands: 33-50 GHz, 60-90 GHz, 90-120 GHz, 140-220 GHz, 220-325 GHz and 325-500 GHz. Due to the wide frequency-range to be covered, it is necessary to implement a multi-frequency source, generating monochromatic amplitude and frequency variable signals and also broadband signals. Another requirement of the calibration source is to provide a very pure linearly polarized signal, presenting a cross-polarization degree of the order of -60 dB. The calibration system proposed in Casas-Reinares et al., 2021 could reduce the uncertainty in polar angle to 1 arc-minute (0.017°) due to the accurate alignment of the source components with the structure of L2-CalSat.

CubeSats and microsatellites have their advantages or disadvantages. In order to know what is the best option depends on how functional, operational and economic requirements fit for a given project. Depending on these criteria, a large number of advantages of CubeSats

over micro-satellites can be found. Or vice versa. It all depends on the type of project it will be carried out. Generally, it is possible to identify some advantages and disadvantages of CubeSats and micro-satellites. Some advantages for CubeSats are the following: more accessible to companies of all types and sizes; shorter development times; more up-to-date technology; modular, scalable, and can be used for different missions and purposes. Some disadvantages are the following: CubeSats have little or no propulsion; so it is difficult to control where they go. Add a propulsion systems means an extra cost; they have a shorter lifespan compared to micro-satellites and can remain in orbit sometimes for no longer than a year. In the other hand, the advantages of micro-satellite missions are considered to be: more frequent mission opportunities and therefore faster return of science and for application data; larger variety of missions and therefore also greater diversification of potential users; more rapid expansion of the technical and/or scientific knowledge base; greater involvement of local and small industry; long operational lifetime in orbit (> 10 years) (Kramer and Cracknell, 2008).

4.2 Calibration signals

The calibration source is expected to cover mainly three 30% bandwidth frequency bands, centred at 40, 90, and 150 GHz. The signals at these three bands will be designed to accomplish both: the observation windows in the atmospheric transmittance spectra, and the spectral bands commonly used in CMB polarimeters. In order to generate calibration signals covering all these frequency bands, it is proposed the use of monochromatic frequency-variable and broadband sources, that can be used to generate variable signals. Each signal would have an associated horn antenna that would emit a coherent linearly polarized beam. The horns produced a small amount of unwanted cross-polarization, and this add uncertainty to the orientation of the calibration signal. In order to decrease this uncertainty, a wire-grid polarizer is installed at the aperture. The final cross-polarization level is less than -60 dB, so 99.9999% of the power in the Calsat signals is emitted in a single polarization orientation. Given that this frequency coverage is not allowed in the Amateur Satellite Service bands in the Table of Frequency Allocations used by the Federal Communications Commission (FCC) and The National Telecommunications and Information Administration (NTIA), it will be needed to ask permission to transmit calibration signals at these frequencies. The signals which are close to the frequencies of interest and we can transmit without require a special permission are described in (DoC, 2021), and have been summarized in the Table 7.

	Frequency bandwidth [GHz]			
Amateur-Satellite	47 - 47.2	79 - 81	134 - 141	241 - 250

Table 7: Frequencies bandwidth in which is allow transmit signals without require special permission by FFC and NTIA.

Notice that in Table 7, the widest band-width is presented near the 250 GHz frequency, which is another frequency commonly used in the CMB detectors to characterize the thermal emission from the interstellar dust. Nevertheless, in this study is not taken into account given the necessity to optimise volume, cost and power consumption of the CalSat.

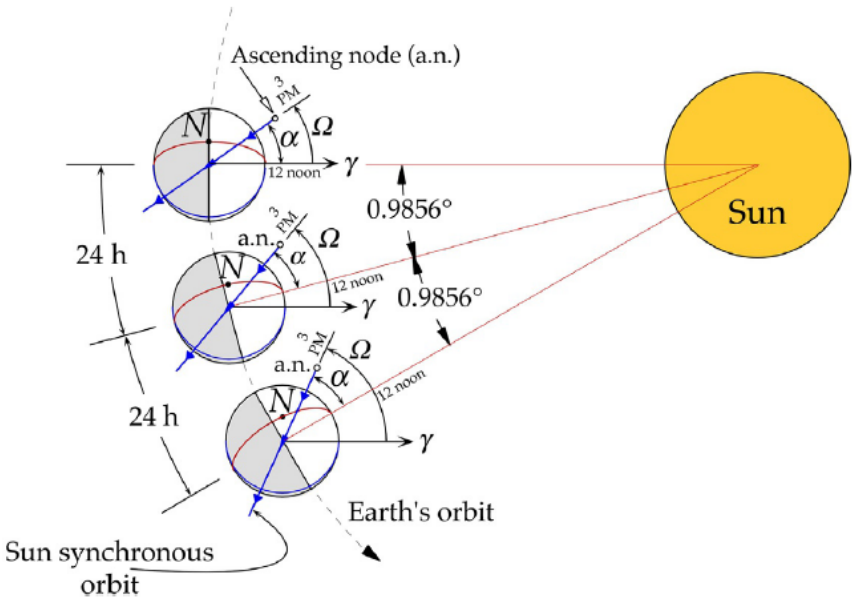

Figure 12: *Visualization of a sun-synchronous orbit. The angle α remains constant and the RAAN (Ω) of the orbit should change 360° per year, thus rotating the orbital plane 0.9856° per day. From Curtis, 2020.*

4.3 Calibration Strategy

4.3.1 Sun-synchronous orbit condition

The proposed Calsat will be placed in a sun-synchronous orbit. Sun-synchronous orbits are those whose orbital plane makes a constant angle α with the radial from the sun, as illustrated in Fig. 12. This can be achieved when the precession rate $\dot{\Omega}$ equals to the mean motion of the Earth around the Sun, which is 360° per 365.26 days, or 0.9856° per day. While the CalSat orbits in a nearly south-north direction, the Earth moves beneath it in a west-east direction, as we can see in Fig. 13. A sun-synchronous orbit does not ensure a good visibility from experiments located in the poles. In our case (altitude = 400 km) CalSat would be visible at a maximum elevation angle of about 23°, as can be seen in the Fig. 14. We can observe in the plot that increasing the altitude of the Calsat, the elevation angle also tends to increase. Therefore, in order to have an adequate visibility of the satellite from experiments on the poles, a higher orbit altitude would be necessary.

The earth is an oblate spheroid and this oblateness causes the right ascension of the ascending node (RAAN) Ω and the argument of periapsis ω to vary significantly with time. The equation which describe the average rate of change of the Ω angle is

$$\dot{\Omega} = -\left[\frac{3\sqrt{\mu}J_2R^2}{2(1-e^2)^2a^{7/2}}\right]\cos i, \tag{6}$$

where, R is radius of the planet, μ is the gravitational parameter (398600.440 km^3/s^2 for Earth); a and e are the semi-major axis and eccentricity of the orbit, respectively; i is the

orbit's inclination and J_2 is the coefficient for the second zonal term related to the oblateness of the planet (1.08263×10^{-3} for Earth).

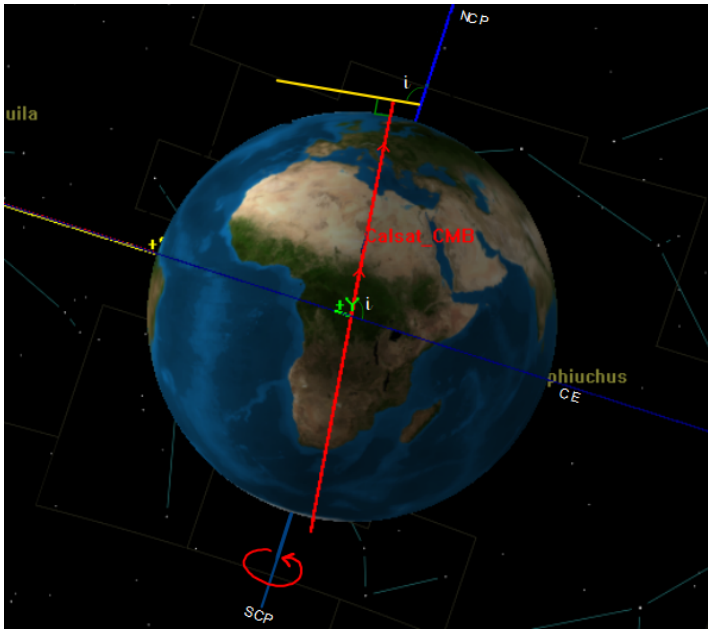

Figure 13: *Conceptual diagram of the sun-synchronous orbit. In this diagram the red line shows the orbital plane of the CalSat, the blue line crossing the Earth (cutting in two halves) is the Celestial Equator (CE). The inclination i is the angle measured by these two planes. The blue line passing through the Earth, is the North and South celestial poles (NCP and SCP, respectively).*

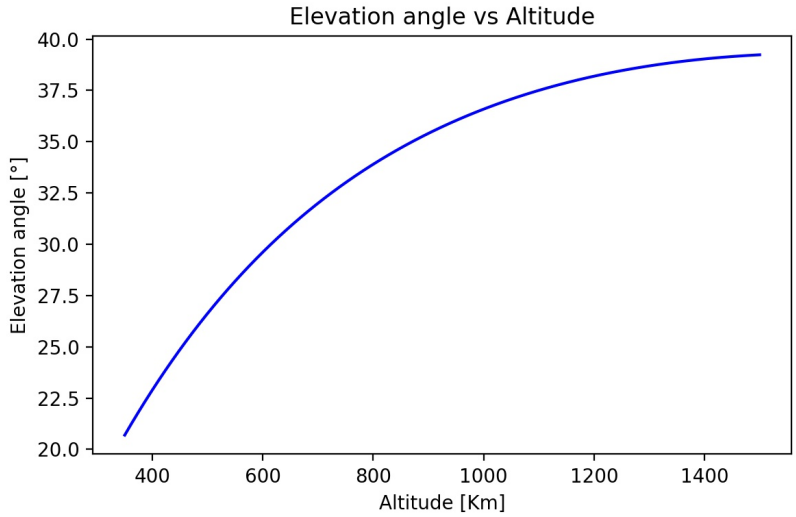

Figure 14: *Elevation angle of a satellite measured by an observer in a pole as a function of the orbit altitude.*

The orbital period can be calculated using the following equation:

$$T = 2\pi\sqrt{\frac{a^3}{\mu}} \tag{7}$$

Using the Eq. 6, and assuming a circular orbit ($e \approx 0$), we can solve for the inclination and find a direct relation between the inclination i and the altitude h, as following:

$$\cos i = \frac{2\dot{\Omega}}{3J_2R^2\sqrt{\mu}} \cdot (h+R)^{7/2}, \tag{8}$$

where h is the orbit altitude ($h = a - R$).
In the Fig. 15 is show the Sun-Synchronous condition, where we have used the Eq. 8. As we can see, as orbit altitude increases, inclination also increases in an almost lineal relation.

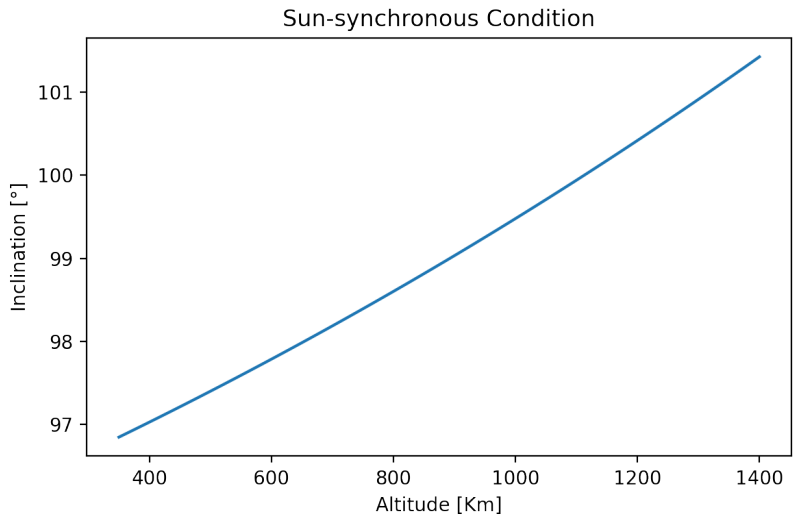

Figure 15: *Sun-synchronous condition: inclination vs altitude, where we have considered the radius of Earth as 6378 km, the eccentricity as 0, and the constant values described in the text.*

In our case, for the SS-CalSat with an orbit altitude of 400 km the corresponding inclination is 97.03°. In the mission design, we selected 400 km as the target altitude for the CalSat given that this is a viable orbit for the new launcher that will be used (Spectrum from ISAR). Using the Eq. 7 we can also calculate the orbital period. For this orbital altitude is 1.54 hr, which means that the CalSat goes around the earth 15.6 times per day.

4.3.2 Visibility

Another interesting fact to know is how many times per week or month the CalSat will pass through the field of view of the experiments and how long will it take. In order to make this calculus, we have used the General Mission Analysis Tool (GMAT) (Hughes, 2016) to

model a dawn-dusk sun-synchronous orbit that was chosen in order to achieve the minimum eclipse time as possible throughout the orbit. In a dawn-to-dusk orbit, the CalSat will trail the Earth's shadow. This allows to the CalSat always has its solar panels facing the sun. To define a sun-synchronous orbit as dawn-dusk we should set the RAAN as 90 degrees during the March equinox. Furthermore the need for a circular orbit, requires an eccentricity with a value as close to zero as possible. The initial parameters for the dawn-dusk sun-synchronous orbit have been established and are shown in Table 8.

The Figs. 16 show the CalSat orbits (for different time lapses) projected on the Earth surface. As we can see, the trajectory trailed in one day does not ensure that the CalSat will pass over the zenith of a given experiment. In a week the CalSat could pass several times over the zenith of any experiment, and for a month we can ensure even more observations in any ground-based experiment (excluding the poles, given the orbit of the CalSat). Therefore, taking into account the coordinates of the CalSat, the position and the field of view from experiments, we can calculate the number of observations per week/month and the time of crossing the field of view. All of this, assuming that the experiments are pointing directly to the zenith.

Parameter	**Value**
Semi-major axis (a)	6778 km
Eccentricity (e)	0.0001
Inclination (i)	97.025°
RAAN($\mathbf{\Omega}$)	90.0°
Argument of perigee (ω)	0°
True anomaly (f)	0°

Table 8: Orbital Parameters of a dawn-dusk SSO at 20th of March 2023.

In the plots in Fig. 17 we can see the orbit trajectories in the field of view of the different experiments. As we can note, the observations of the CalSat depends of the FOV. For the the experiments with a small FOV (as ACT), the observations are fewer than the observations for experiments with a bigger FOV (as CLASS or QUBIC). For example, in the case of ACT the observations are just four in one month. Nevertheless, for CLASS or QUBIC we have a lot of observations, and in most of the cases we can observe the CalSat more than one time per day. Also, given the symmetry of the pattern of the trajectories of the CalSat in the sky, as we can see in Fig. 16 d), the observations depends more of the FOV than the location of the experiment.

In Table 9, we can see the observations over one month for each experiment and a summary about the observation times. Note that, we have taken into account each observation as each in and out trajectory of the FOV. Therefore, when the CalSat pass over the FOV several times per day, we have counted each crossing as an observation. CLASS presents the largest number of observations, therefore the largest observing time. Given the small FOV of ACT, the number of observations in one month is just four times and with little time (maximum duration of 14 s). Therefore, this calibration system should be carefully applied for experiments with small FOV. In this case, could be better to implement a CalSat tracking within the telescope scan strategy in order to achieve a properly calibration.

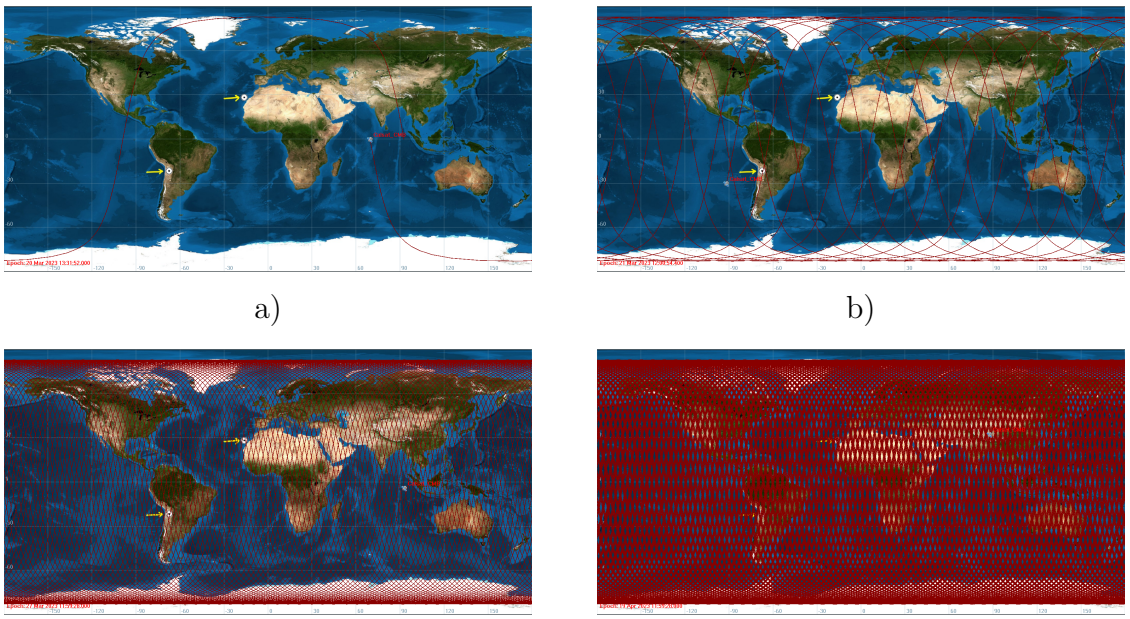

Figure 16: CalSat orbits projected on Earth (in red lines) for a) 1.54 hr, b) one day, c) 7 days, and d) 30 days. The experiments of our interest are marked with a black point surrounded by a circle.

Experiment	Number of observations	Minimum duration [s]	Maximum duration [s]	Mean duration [s]	Total duration [s]	FOV [°]
CLASS	41	74	241	195	7992	16
QUBIC	34	100	194	158	5382	13
ACT	4	5	14	10.5	42	1
LSPE-STRIP	14	24	74	59	830	5
QUIJOTE	20	28	120	97	1943	8

Table 9: *Number of observations in one month and information about the observation time for each experiment.*

5 Thermal Control

A model simulation implemented in the `ASATAN` software, shows that a maximum temperature of 39° C is reached in part of the surface of the solar panels that is facing the sun (Casas-Reinares et al., 2021). Taking this value as the temperature reached by the whole panels, the solar panels radiate thermal emission which is absorbed by the detectors in the experiments and this radiation could saturate them. Table 10 shows the absorbed power and the saturation power for the ground-based experiments of interest, where we have consider to cover experiments with small and large apertures. As we can see, in the extreme case, where the aperture is 6 meters (ACT) and in a frequency of 240 GHz, the radiation absorbed

is about 7.5×10^{-3} pW, that is about more than 3 orders of magnitude lower than the saturation power of the detectors (25 pW) at the same frequency in ACT. Furthermore, we can see in Table 10 that the thermal emission from the calibration satellite does not saturate any frequency band detectors on any experiment.

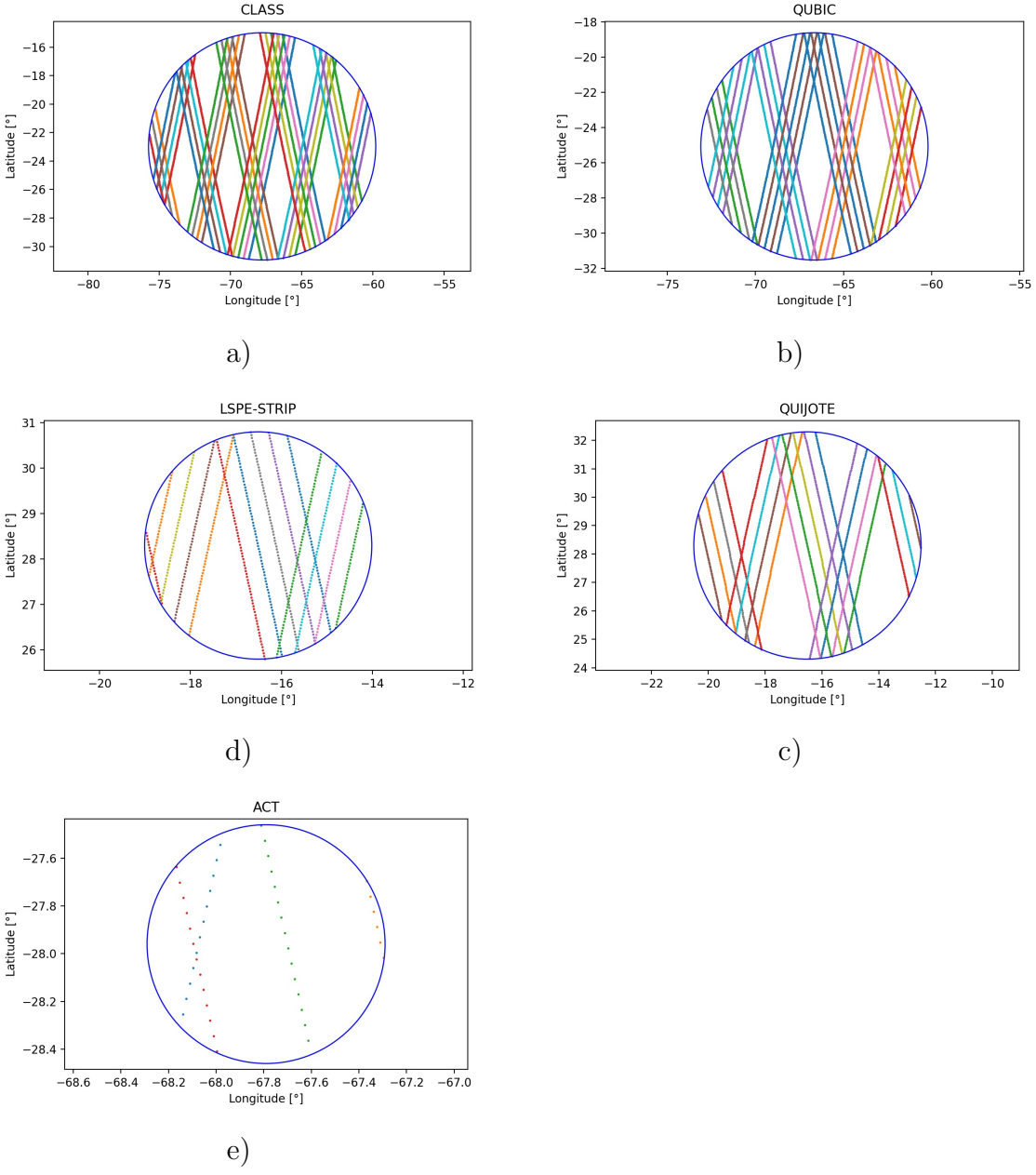

Figure 17: *CalSat trajectories for each experiment, where we have considered the observation time as one month, and the respective FOV for the experiments. The lines constructed by the points represent the trajectories of the CalSat and the 'lines' with same colour represent the same observing day.*

The absorbed power by the experiments detectors due to the thermal emission emitted by the solar panels is calculated using the Eq. 9 as following,

$$P_{ab}(Th) = \frac{1}{6}\frac{A_r}{c^2}k_B\left(3\epsilon + \frac{\epsilon^3}{4}\right)\nu^3\left(\frac{A_p/2}{d}\right)^2 T, \tag{9}$$

where A_r is the reflective area of the solar panels, c is the light speed, K_B is the Boltzmann constant, ϵ is the relative band width, ν is the frequency, A_p is the telescope aperture, d is the distance between the Calsat and the ground-based experiment, and T is the temperature on the surface of the panels. It has been assumed the worst case scenario where the temperature of the CalSat is the maximum temperature reached by the solar panels and this panels (four solar panels with dimensions 60×50 cm) are facing perfectly the telescope aperture. The central frequency and relative bandwidth is also taken into account, as well as the distance Calsat-Ground-based experiment which is 400 km. The saturation power for CLASS are calculated in (Dahal et al., 2022), for Advanced ACT in (Henderson et al., 2016; Choi et al., 2018; Li et al., 2018). In the cases for QUBIC, QUIJOTE and LSPE-STRIP we use an indirect method where the Detector Noise Temperature (NET) and bandwidth is used to calculate the Noise Power (P_N) using the following equation:

$$P_N = K_B(NET)B^{(3/2)}, \tag{10}$$

where B is the bandwidth and K_B is the Boltzmann constant. Using the Eq. 10 we can calculate the saturation power taking into account that $P_{sat} \approx 10P_N$. The NET values for QUBIC are calculated in (Hamilton et al., 2022), for QUIJOTE in (López-Caniego et al., 2014), and for LSPE-STRIP in (Addamo et al., 2021).

Experiment	**Frequency [GHz]**							
	40		**90**		**150**		**240**	
	$P_{ab}(Th)$	P_{sat}	$P_{ab}(Th)$	P_{sat}	$P_{ab}(Th)$	P_{sat}	$P_{ab}(Th)$	P_{sat}
QUBIC	-	-	-	-	1.2×10^{-5}	1.1×10^{2}	5.5×10^{-5}	3.0×10^{2}
CLASS	1.0×10^{-7}	6.3	3.6×10^{-6}	18.4	2.0×10^{-5}	35.0	5.9×10^{-5}	43.8
LSPE-STRIP	1.2×10^{-6}	44	5.9×10^{-6}	1.0×10^{2}	-	-	-	-
QUIJOTE	3.7×10^{-6}	62	-	-	-	-	-	-
AdvACT	5.1×10^{-5}	7.8	5.1×10^{-4}	14	1.5×10^{-3}	15	7.5×10^{-3}	25

Table 10: *Absorbed power and saturation power by the detectors, for the different experiments and frequencies. All the power values are in pW.*

Another CalSat component which could saturate the experiment detectors is the horn antennas (these are the ones that transmit the polarized signals) due to the thermal emission from them. In order to calculate the absorbed power by the experiments from this spurious signal, the equation 9 is used again. For instance, the absorbed power as a function of the temperature has been calculated. We have considered the experiment with the largest aperture (in this work, ACT) and each frequency band at which ACT detects signals. Also, the proposed calibration source from CalSat would count with three frequency bands. Hence, it is necessary three antennas to cover them. The size of the antennas, mainly depends of the frequency at which these transmit. For instance, we concern about the antennas diameter, which have been taken as the reflecting area. The diameter of the antennas for the three

frequency bands are the following: (33 - 50 GHz, 108 mm), (75 - 110 GHz, 53 mm) and (110 - 170 GHz, 37 mm) [1]. In Fig. 18 we can see the absorbed power by the ACT experiment from the thermal emission of CalSat antennas as a function of the temperature. We have considered as the upper limit the extreme scenario where the temperature reach about 200 °C (extreme given that the solar panels reach a maximum temperature of 39°C). We can note in the Table 10 that the saturation power in the highest frequency for ACT is 25 pW and from Fig. 18 the absorbed power in the extreme scenario (200 °C, 220 GHz) is about 1.2×10^{-4} pW. Therefore, even in this extreme scenario the thermal emission form CalSat antennas does not saturate the ACT detectors (including those that detect at a lower frequency). In addition, given that the others experiments studied in this work, count with aperture less than ACT, these will not saturate either.

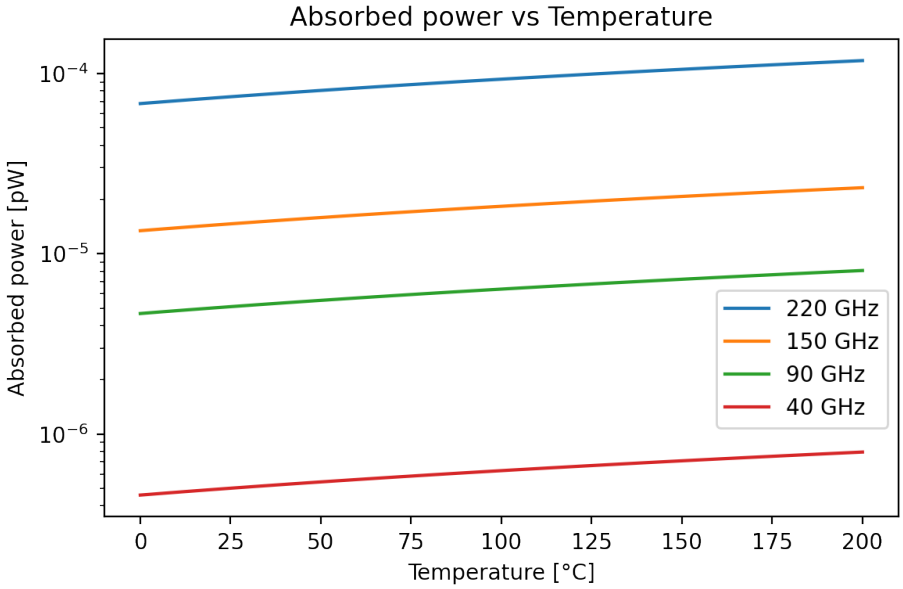

Figure 18: *Absorbed power by the ACT experiment from the thermal emission of the horn antennas as a function of the temperature. It has been considered each frequency band at which ACT detects.*

6 Conclusions

A description of the main characteristics of a calibration satellite for groun-based CMB polarization experiments, has been carried out. The CalSat is expected to be used for the calibration of ground-based experiments mainly located in Tenerife and Atacama, with small and large aperture. The visibility of the CalSat with the calibration strategy implemented in this work (the experiments calibrate observing at zenith), depends mainly of the FOV of a given experiment. In experiments with a small FOV the calibration system should be carefully applied, given the little observation time (a mean of 10.5 s). In these cases a CalSat tracking could ensure a better observation time. The CalSat visibility from the poles exper-

[1] https://anteral.com/products/lha-lens-horn-antennas/

iments (taking into account the orbit altitude of 400 km in a SSO) counts with a maximum elevation of about 23°, which could be challenging for a calibration given the characteristics of the experiments and the atmospheric effects. In order to improve this visibility and cover experiments located in poles, a higher orbit altitude has to be implemented.
The calibration source frequencies are expected to be centred at 40, 90 and 150 GHz. Nevertheless, another frequency of interest is 250 GHz, this is needed to characterize the interstellar dust and this frequency coverage is allowed by the FCC and NTIA. Therefore, it would be necessary add this frequency band in a future design.
Taking into account the maximum temperature reached by the surface of the solar panels of the CalSat and the calculated absorbed power, the thermal radiation emitted does not saturate the experiments detectors, even for experiments with large aperture.

The CalSat would reduce the polar angle error to the level of 1 arc-minute thanks to the cross-polarization level less than -60 db and a very good knowledge of the calibration signals. Also, it would allow the characterization of both, the intensity and polarization optical main beam. The level of accuracy reached by means the CalSat is not available using natural sources given that the best option allows an accuracy for the polarization orientation up to 0.5°. On the other hand, the level of sensitivity reached using the CalSat will allow outstanding scientific results to be achieved in current and future CMB experiments.

References

Abitbol, M. H., Hill, J. C., & Johnson, B. R. (2016). Foreground-induced biases in CMB polarimeter self-calibration. *Monthly Notices of the Royal Astronomical Society*, *457*(2), 1796–1803. https://doi.org/10.1093/mnras/stw030

Addamo, G., Ade, P., Baccigalupi, C., Baldini, A., Battaglia, P., Battistelli, E., Baù, A., De Bernardis, P., Bersanelli, M., Biasotti, M., et al. (2021). The large scale polarization explorer (lspe) for cmb measurements: Performance forecast. *Journal of Cosmology and Astroparticle Physics*, *2021*(08), 008.

Ade, P. A. R., Ahmed, Z., Amiri, M., Barkats, D., Thakur, R. B., Bischoff, C. A., Beck, D., Bock, J. J., Boenish, H., Bullock, E., Buza, V., Cheshire, J. R., Connors, J., Cornelison, J., Crumrine, M., Cukierman, A., Denison, E. V., Dierickx, M., Duband, L., ... Zhang, S. (2021). Improved constraints on primordial gravitational waves using planck, wmap, and bicep/keck observations through the 2018 observing season. *Phys. Rev. Lett.*, *127*, 151301. https://doi.org/10.1103/PhysRevLett.127.151301

Aumont, J., Macıéas-Pérez, J. F., Ritacco, A., Ponthieu, N., & Mangilli, A. (2020). Absolute calibration of the polarisation angle for future cmb b-mode experiments from current and future measurements of the crab nebula. *Astronomy & Astrophysics*, *634*, A100.

Baumann, D., Jackson, M. G., Adshead, P., Amblard, A., Ashoorioon, A., Bartolo, N., Bean, R., Beltrán, M., De Bernardis, F., Bird, S., et al. (2009). Probing inflation with cmb polarization. *AIP Conference Proceedings*, *1141*(1), 10–120.

Bigot-Sazy, M.-A., Charlassier, R., Hamilton, J.-C., Kaplan, J., & Zahariade, G. (2013). Self-calibration: An efficient method to control systematic effects in bolometric interferometry. *Astronomy & Astrophysics*, *550*, A59.

Bock, J., Church, S., Devlin, M., Hinshaw, G., Lange, A., Lee, A., Page, L., Partridge, B., Ruhl, J., Tegmark, M., et al. (2006). Task force on cosmic microwave background research. *arXiv preprint astro-ph/0604101*.

Casas-Reinares, F., Martıénez-González, E., Bermejo-Ballesteros, J., Garcıéa-González, S., Cubas, J., Vielva, P., Barreiro, R. B., & Sanz-Andres, A. (2021). L2-calsat: A calibration satellite for ultra-sensitive cmb polarization space missions.

Choi, S. K., Austermann, J., Beall, J. A., Crowley, K. T., Datta, R., Duff, S. M., Gallardo, P. A., Ho, S., Hubmayr, J., Koopman, B. J., et al. (2018). Characterization of the mid-frequency arrays for advanced actpol. *Journal of Low Temperature Physics*, *193*(3), 267–275.

Curtis, H. (2020). *Orbital mechanics for engineering students: Revised reprint*. Butterworth-Heinemann.

Dahal, S., Appel, J. W., Datta, R., Brewer, M. K., Ali, A., Bennett, C. L., Bustos, R., Chan, M., Chuss, D. T., Cleary, J., et al. (2022). Four-year cosmology large angular scale surveyor (class) observations: On-sky receiver performance at 40, 90, 150, and 220 ghz frequency bands. *The Astrophysical Journal*, *926*(1), 33.

Delabrouille, J., Betoule, M., Melin, J.-B., Miville-Deschênes, M.-A., Gonzalez-Nuevo, J., Le Jeune, M., Castex, G., de Zotti, G., Basak, S., Ashdown, M., Aumont,

J., Baccigalupi, C., Banday, A. J., Bernard, J.-P., Bouchet, F. R., Clements, D. L., da Silva, A., Dickinson, C., Dodu, F., ... Toffolatti, L. (2013). The pre-launch planck sky model: A model of sky emission at submillimetre to centimetre wavelengths. *A&A*, *553*, A96. https://doi.org/10.1051/0004-6361/201220019

DoC, N. (2021). Manual of regulations and procedures for federal radio frequency management. *NTIA*.

Fowler, J., Niemack, M., Dicker, S., Aboobaker, A., Ade, P. A., Battistelli, E., Devlin, M., Fisher, R., Halpern, M., Hargrave, P., et al. (2007). Optical design of the atacama cosmology telescope and the millimeter bolometric array camera. *Applied optics*, *46*(17), 3444–3454.

Hamilton, J.-C., Mousset, L., Battistelli, E., De Bernardis, P., Bigot-Sazy, M.-A., Chanial, P., Charlassier, R., D'Alessandro, G., De Petris, M., Lerena, M. G., et al. (2022). Qubic i: Overview and science program. *Journal of Cosmology and Astroparticle Physics*, *2022*(04), 034.

Harrington, K., Marriage, T., Ali, A., Appel, J. W., Bennett, C. L., Boone, F., Brewer, M., Chan, M., Chuss, D. T., Colazo, F., Dahal, S., Denis, K., Dünner, R., Eimer, J., Essinger-Hileman, T., Fluxa, P., Halpern, M., Hilton, G., Hinshaw, G. F., ... Zeng, L. (2016). The Cosmology Large Angular Scale Surveyor. In W. S. Holland & J. Zmuidzinas (Eds.), *Millimeter, submillimeter, and far-infrared detectors and instrumentation for astronomy viii* (99141K). https://doi.org/10.1117/12.2233125

Henderson, S., Allison, R., Austermann, J., Baildon, T., Battaglia, N., Beall, J., Becker, D., De Bernardis, F., Bond, J., Calabrese, E., et al. (2016). Advanced actpol cryogenic detector arrays and readout. *Journal of Low Temperature Physics*, *184*(3), 772–779.

Hoyland, R. J., Aguiar-González, M., Aja, B., Ariño, J., Artal, E., Barreiro, R., Blackhurst, E., Cagigas, J., De Diego, J. C., Casas, F., et al. (2012). The status of the quijote multifrequency instrument. *Millimeter, Submillimeter, and Far-Infrared Detectors and Instrumentation for Astronomy VI*, *8452*, 935–949.

Hughes, S. P. (2016). *General mission analysis tool (gmat)* (tech. rep.).

Johnson, B. R., Vourch, C. J., Drysdale, T. D., Kalman, A., Fujikawa, S., Keating, B., & Kaufman, J. (2015). A cubesat for calibrating ground-based and sub-orbital millimeter-wave polarimeters (calsat). *Journal of Astronomical Instrumentation*, *4*(03n04), 1550007.

Johnstone, A. (2020). Cubesat design specification (1u-12u) rev 14 cp-cds-r14. *The CubeSat Program, Cal Poly SLO, July*.

Jungman, G., Kamionkowski, M., Kosowsky, A., & Spergel, D. N. (1996). Cosmological-parameter determination with microwave background maps. *Physical Review D*, *54*(2), 1332.

Kamionkowski, M., Kosowsky, A., & Stebbins, A. (1997). Statistics of cosmic microwave background polarization. *Physical Review D*, *55*(12), 7368.

Keating, B. G., Shimon, M., & Yadav, A. P. (2012). Self-calibration of cosmic microwave background polarization experiments. *The Astrophysical Journal Letters*, *762*(2), L23.

Koopman, B., Austermann, J., Cho, H.-M., Coughlin, K. P., Duff, S. M., Gallardo, P. A., Hasselfield, M., Henderson, S. W., Ho, S.-P. P., Hubmayr, J., et al. (2016). Optical modeling and polarization calibration for cmb measurements with actpol and advanced actpol. *Millimeter, Submillimeter, and Far-Infrared Detectors and Instrumentation for Astronomy VIII*, *9914*, 687–698.

Kramer, H. J., & Cracknell, A. P. (2008). An overview of small satellites in remote sensing. *International journal of remote Sensing*, *29*(15), 4285–4337.

Lamagna, L., Addamo, G., Ade, P., Baccigalupi, C., Baldini, A., Battaglia, P., Battistelli, E., Baù, A., Bersanelli, M., Biasotti, M., et al. (2020). Progress report on the large-scale polarization explorer. *Journal of Low Temperature Physics*, *200*(5), 374–383.

Lee, A. T., Ade, P., Akiba, Y., Alonso, D., Arnold, K., Aumont, J., Austermann, J., Baccigalupi, C., Banday, A., Banerji, R., et al. (2019). Litebird: An all-sky cosmic microwave background probe of inflation. *Bulletin of the American Astronomical Society*, *51*(GSFC-E-DAA-TN74209).

Li, Y., Austermann, J. E., Beall, J. A., Bruno, S. M., Choi, S. K., Cothard, N. F., Crowley, K. T., Duff, S. M., Gallardo, P. A., Henderson, S. W., et al. (2018). Performance of the advanced actpol low frequency array. *Millimeter, Submillimeter, and Far-Infrared Detectors and Instrumentation for Astronomy IX*, *10708*, 16–24.

López-Caniego, M., Rebolo, R., Aguiar, M., Génova-Santos, R., Gómez-Reñasco, F., Gutierrez, C., Herreros, J., Hoyland, R., López-Caraballo, C., Santos, A., et al. (2014). The quijote cmb experiment: Status and first results with the multi-frequency instrument. *arXiv preprint arXiv:1401.4690*.

Mele, L., Ade, P., Alberro, J. G., Almela, A., Amico, G., Arnaldi, L. H., Auguste, D., Aumont, J., Azzoni, S., Banfi, S., Battistelli, E. S., Baù, A., Bèlier, B., Bennett, D., Bergé, L., Bernard, J.-P., Bersanelli, M., Bigot-Sazy, M.-A., Bleurvacq, N., … Zullo, A. (2020). The QUBIC instrument for CMB polarization measurements. *Journal of Physics: Conference Series*, *1548*(1), 012016. https://doi.org/10.1088/1742-6596/1548/1/012016

Nati, F., Devlin, M. J., Gerbino, M., Johnson, B. R., Keating, B., Pagano, L., & Teply, G. (2017). Polocalc: A novel method to measure the absolute polarization orientation of the cosmic microwave background. *Journal of Astronomical Instrumentation*, *6*(02), 1740008.

O'Sullivan, C., De Petris, M., Amico, G., Battistelli, E., de Bernardis, P., Burke, D., Buzi, D., Chapron, C., Conversi, L., D'Alessandro, G., et al. (2022). Qubic viii: Optical design and performance. *Journal of Cosmology and Astroparticle Physics*, *2022*(04), 041.

Page, L., Hinshaw, G., Komatsu, E., Nolta, M. R., Spergel, D. N., Bennett, C. L., Barnes, C., Bean, R., Doré, O., Dunkley, J., Halpern, M., Hill, R. S., Jarosik, N., Kogut, A., Limon, M., Meyer, S. S., Odegard, N., Peiris, H. V., Tucker, G. S., … Wright, E. L. (2006). Three year wilkinson microwave anisotropy probe (wmap) observations: Polarization analysis.

Poidevin, F., Rubino-Martin, J., Genova-Santos, R., Rebolo, R., Aguiar, M., Gomez-Renasco, F., Gutierrez, C., Hoyland, R., Lopez-Caraballo, C., Carreras, A. O., et al. (2018). The quijote experiment: Prospects for cmb b-mode polarization detection and foregrounds characterization. *arXiv preprint arXiv:1802.04594*.

Rubiño-Martín, J. A., Rebolo, R., Aguiar, M., Génova-Santos, R., Gómez-Reñasco, F., Herreros, J., Hoyland, R., López-Caraballo, C., Santos, A. P., De La Rosa, V. S., et al. (2012). The quijote-cmb experiment: Studying the polarisation of the galactic and cosmological microwave emissions. *Ground-based and Airborne Telescopes IV*, *8444*, 987–997.

Rubiño-Martín, J. A., Rebolo, R., Tucci, M., Genova-Santos, R., Hildebrandt, S., Hoyland, R., Herreros, J., Gomez-Renasco, F., Caraballo, C. L., Martinez-Gonzalez, E., et al. (2010). The quijote cmb experiment. In *Highlights of spanish astrophysics v* (pp. 127–135). Springer.

The CMB-S4 Collaboration, K. N., Abazajian, Adshead, P., Ahmed, Z., Allen, S. W., Alonso, D., Arnold, K. S., Baccigalupi, C., Bartlett, J. G., Battaglia, N., Benson, B. A., et al. (2016). Cmb-s4 science book. *arXiv preprint arXiv:1610.02743*.

Thornton, R., Ade, P., Aiola, S., Angile, F., Amiri, M., Beall, J., Becker, D., Cho, H., Choi, S., Corlies, P., et al. (2016). The atacama cosmology telescope: The polarization-sensitive actpol instrument. *The Astrophysical Journal Supplement Series*, *227*(2), 21.

Zaldarriaga, M., & Seljak, U. (1997). All-sky analysis of polarization in the microwave background. *Physical Review D*, *55*(4), 1830–1840. https://doi.org/10.1103/physrevd.55.1830